IOP PUBLISHING ENVIRONMENTAL RESEARCH LETTERS
Environ. Res. Lett. **2** (2007) 045015 (9pp) doi:10.1088/1748-9326/2/4/045015

Methane emissions from western Siberian wetlands: heterogeneity and sensitivity to climate change

T J Bohn[1], D P Lettenmaier[1], K Sathulur[2], L C Bowling[2], E Podest[3], K C McDonald[3] and T Friborg[4]

[1] Department of Civil and Environmental Engineering, University of Washington, Seattle, WA, USA
[2] Department of Agronomy, Purdue University, West Lafayette, IN, USA
[3] Water and Carbon Cycles Group, Earth Sciences Division, NASA Jet Propulsion Laboratory, Pasadena, CA, USA
[4] Department of Geography and Geology, University of Copenhagen, Copenhagen, Denmark

Received 21 June 2007
Accepted for publication 10 September 2007
Published 26 November 2007
Online at stacks.iop.org/ERL/2/045015

Abstract
The prediction of methane emissions from high-latitude wetlands is important given concerns about their sensitivity to a warming climate. As a basis for the prediction of wetland methane emissions at regional scales, we coupled the variable infiltration capacity macroscale hydrological model (VIC) with the biosphere–energy-transfer–hydrology terrestrial ecosystem model (BETHY) and a wetland methane emissions model to make large-scale estimates of methane emissions as a function of soil temperature, water table depth, and net primary productivity (NPP), with a parameterization of the sub-grid heterogeneity of the water table depth based on TOPMODEL. We simulated the methane emissions from a 100 km × 100 km region of western Siberia surrounding the Bakchar Bog, for a retrospective baseline period of 1980–1999 and have evaluated their sensitivity to increases in temperature of 0–5 °C and increases in precipitation of 0–15%. The interactions of temperature and precipitation, through their effects on the water table depth, played an important role in determining methane emissions from these wetlands. The balance between these effects varied spatially, and their net effect depended in part on sub-grid topographic heterogeneity. Higher temperatures alone increased methane production in saturated areas, but caused those saturated areas to shrink in extent, resulting in a net reduction in methane emissions. Higher precipitation alone raised water tables and expanded the saturated area, resulting in a net increase in methane emissions. Combining a temperature increase of 3 °C and an increase of 10% in precipitation to represent climate conditions that may pertain in western Siberia at the end of this century resulted in roughly a doubling in annual emissions.

Keywords: bog, methane, peatland, wetland, VIC, hydrology, model, TOPMODEL, topographic wetness index, BETHY, spatial distribution, climate, Siberia, Bakchar, Vasyugan, sensitivity, heterogeneity

1. Introduction

Wetlands play an important dual role in the global carbon cycle as both the largest natural methane source (115 Tg CH_4 y^{-1}; Matthews and Fung 1987) and a large net carbon sink (76 Tg C y^{-1} for high-latitude peatlands alone; Gorham 1991). Both the extent of wetlands and the balance between their methane emissions and carbon sequestration depend on climatological and hydrological factors, leading to potentially significant feedbacks to the global climate system. This is

especially true in the northern high latitudes, where ongoing and projected climate change is most pronounced (Serreze *et al* 2000, IPCC 2007), and particularly so in northern Eurasia, where roughly 30% of global wetlands are found (Matthews and Fung 1987, Gorham 1991). Despite the importance of these systems to the global carbon cycle, substantial uncertainties remain in estimates of their extents, carbon fluxes, and responses to climate change. This is due in large part to the sparseness of *in situ* observations in northern Eurasia.

Field studies have shown that wetland methane emissions depend on a number of environmental factors, among the most important of which are soil temperature, water table depth, and substrate (organic carbon) quality (e.g. Dise *et al* 1993, Shannon and White 1994, Valentine *et al* 1994, Panikov and Dedysh 2000). In a review of field studies, Christensen *et al* (2003) found that the dependence of methane emissions on water table depth is highly non-linear. When the water table is within roughly 10 cm of the surface, soil temperature becomes the limiting factor on methane production and sensitivity to the water table becomes small. Below a depth of 10 cm, water table depth quickly becomes the limiting factor. In addition, while temperature drives methane emissions through its control on metabolic rates, it also influences the water table depth indirectly through snow melt and evapotranspiration. Simulations of future climate suggest that western Siberia may become wetter and warmer (IPCC 2007) over the next century. The resulting water table depths, and, in turn, wetland methane emissions, could rise or fall depending on the balance between increasing precipitation and higher temperatures.

In addition, soil moisture storage can be highly heterogeneous, due mostly to microtopographic effects (e.g. Famiglietti *et al* 1998, Famiglietti *et al* 1999). This raises the question of whether water tables at sites where methane emissions have been measured are representative of the wetlands in the surrounding region, especially in the case of large wetland complexes such as those found in western Siberia, where measurements from only a handful of sites have been published. Indeed, wetland methane emissions have been found to vary considerably along transects of only a few hundred metres (e.g. Panikov and Dedysh 2000, Saarnio *et al* 1997), often as a result of variations in water table depth associated with local topographic features. Thus, it is reasonable to suppose that the areal extent of methane-emitting regions across the landscape, and therefore total methane emissions, are a function of the spatial distribution of water table depths.

Large-scale modeling offers a means of understanding these interactions across the landscape in the face of sparse observations. To predict the response of global wetland methane emissions to future climate, several large-scale modeling studies have been performed (e.g. Zhuang *et al* 2006, Gedney *et al* 2004, Shindell *et al* 2004), the consensus of which is that northern wetland methane emissions will at least double by the end of the 21st century. Of these, only Gedney *et al* considered the sub-grid heterogeneity of the water table. They found that wetland extent did not increase substantially under future predicted climate, and that the primary driver of increased methane emissions was increased temperature. However, they applied their model globally over a coarse (2.5° × 3.75°) grid, and calibrated it against global interannual variability in atmospheric methane concentrations. On the other hand, Shindell *et al* found that increases in wetland extent played a major role in increasing emissions; however, they only considered average water table depths over a coarse (1° × 1°) grid.

In this study, we investigate the response of northern wetlands to changes in climate by applying a macroscale hydrological and biogeochemical model with a parameterization of sub-grid heterogeneity of the water table depth over a 100 km × 100 km region of western Siberia. After calibrating with local observations of water table depth and methane emissions, we examine the effects of increased temperature and increased precipitation, both separately and in conjunction, on the spatial distribution of water table depths and the resulting distribution of methane emissions over the region.

2. Methods

Our study region consists of a single 100 km × 100 km grid cell (from the EASE grid equal area projection; Brodzik and Knowles 2002) centered at 56° 29′ N, 83° 09′ E, near the town of Plotnikovo in western Siberia (see figure 1). This grid cell contains the Bakchar Bog, a roughly 15 km × 30 km portion of the large Vasyugan wetlands complex, where several research teams (e.g. Panikov and Dedysh 2000, Panikov *et al* 2001, Friborg *et al* 2003) sampled methane emissions throughout the 1990s. The sample site (56° 51′ N, 82° 50′ E) is located near the edge of the bog, just outside a network of drainage canals.

Our modeling framework couples the variable infiltration capacity macroscale hydrology model (VIC; Liang *et al* 1994) with the biosphere–energy-transfer–hydrology terrestrial ecosystem model (BETHY; Knorr 2000) and the wetland methane emissions model of Walter and Heimann (2000). Following the standard VIC protocol, each grid cell in the domain (a single cell in this case) consists of a horizontally uniform, multi-layer soil column overlain by a mosaic of landcover 'tiles'. For each tile, given meteorological observations as input, VIC solves the moisture and energy balances for the land surface at an hourly time step, tracking soil moisture and temperature profiles, snow water equivalent, transpiration, and soil freezing depth. Since the study region lies outside the southernmost extent of Eurasian permafrost, permafrost dynamics are not simulated. Similarly, the BETHY component computes hourly net primary productivity (NPP) via a Farquhar formulation (Farquhar *et al* 1980), given meteorological fluxes and VIC's soil moisture and temperature. Stomatal conductances are computed using a resistance-factor approach (Dickinson *et al* 1991) that takes into account evapotranspiration limitations due to temperature, light, vapor pressure deficit, and soil moisture. Nutrient availability is not simulated. Fluxes and storages from the individual tiles are then aggregated to produce grid-cell-average values. Daily average soil temperatures, the distribution of water table depth (see below), and NPP (as a proxy for carbon substrate availability) are provided to the methane model, which simulates methane production below

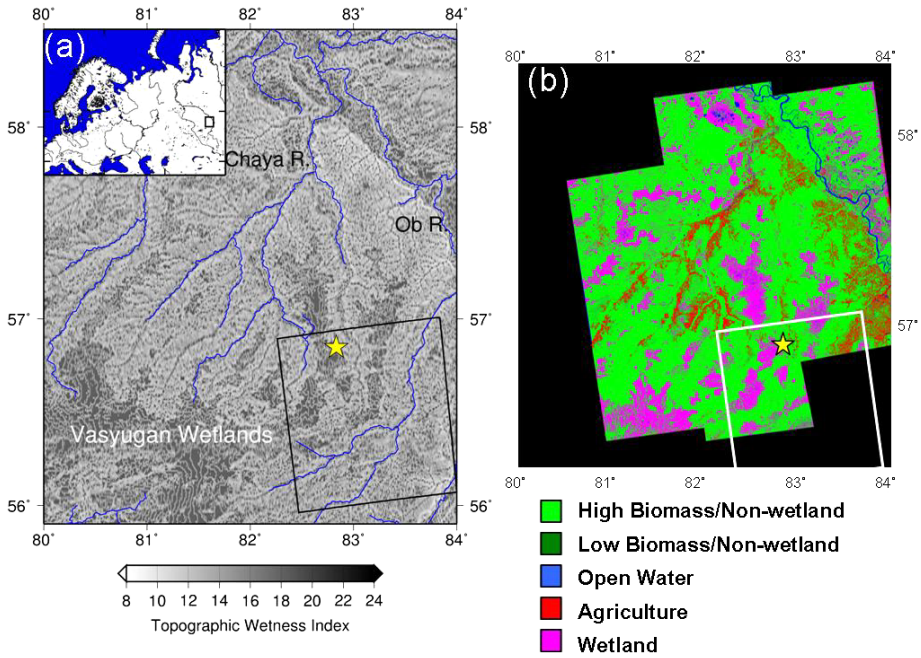

Figure 1. Location of study region. (a) Map of the topographic wetness index, derived from SRTM30 DEM (Farr and Kobrick 2000), over the region. (b) Landcover of the region, derived from random forest (Chen *et al* 2004) classification of ALOS/PALSAR imagery (courtesy of JAXA). In panels (a) and (b), the Bakchar Bog observation site is marked with the yellow star, and the 100 km × 100 km EASE-grid cell centered at (56° 29′ N, 83° 09′ E) is outlined in black (a) and white (b). Note the close correspondence between areas of high topographic wetness index (>14) in panel (a) and areas of wetland in panel (b).

the water table; transport of methane through the soil via diffusion, ebullition, and plant-aided transport; and oxidation above the water table to arrive at an estimate of daily methane emissions.

Among the extensions we have made to the VIC model is a simple scheme to convert the grid-cell-average soil moisture profile into a grid-cell-average water table depth. Our method follows Letts *et al* (2000), with one exception. For each modeled soil layer, we compute the fractional volume of saturated soil Θ_v as

$$\Theta_v = (\theta_i - \theta_r)/(\theta_p - \theta_r) \tag{1}$$

where θ_i is the volumetric moisture of the ith soil layer, θ_p is the porosity of the ith soil layer and θ_r is the residual moisture of the ith soil layer.

Next, the total water table depth z_{WT} is computed as the sum of the moisture deficits of all of the model soil layers:

$$z_{\mathrm{WT}} = \sum_{i=1}^{3} \mathrm{d}z_i(1 - \Theta_{vi}) \tag{2}$$

where $\mathrm{d}z_i$ is the thickness of the ith soil layer.

In Letts *et al* (2000), θ_r in equation (1) represented the specific retention of the ith soil layer, essentially equivalent to the layer's field capacity. Since the hydraulics of the VIC model follow Brooks and Corey (1964), and drainage can continue well beyond field capacity, we were unable to produce results using the Letts *et al* (2000) parameterization for which the soil moisture was greater than specific retention in any layer for more than a short period of time. Therefore, we replaced specific retention with residual moisture in equation (1).

To account for spatial heterogeneity of the water table depth within each grid cell, we employ a relationship between sub-grid topography and local water table depth taken from TOPMODEL (Beven and Kirkby 1979), and incorporate the bias correction of Saulnier and Datin (2004). Sub-grid topography in this case is supplied by the 30-Arc-Second Shuttle Radar Topography Mission (SRTM30) digital elevation model (DEM) (Farr and Kobrick 2000), which has a spatial resolution of 900 m. Under the assumptions that the surface infiltration rate and soil properties are uniform across a basin, and that subsurface transmissivity has an exponential profile with water table depth, the local water table depth z_{WT_i} in pixel i of the DEM at time t can be expressed as a function of the average grid cell water table at time t and grid cell topography as

$$z_{\mathrm{WT}_i}(t) = \overline{z_{\mathrm{WT}}}(t) - m[\kappa_i - \lambda] \tag{3}$$

where m is the scaling parameter, κ_i is the topographic wetness index $= \ln(a_i/\tan\beta_i)$, a_i is the upslope contributing area above location i, $\tan\beta_i$ is the local surface slope and λ is the average of κ_i over the unsaturated area of the grid cell.

The distribution of the topographic wetness index κ_i across the basin depends only on basin topography and is constant in time. Thus, across the basin, the distribution of water table depths over time has the same shape as the distribution of κ_i, but with a time-dependent grid-cell-average value given by the VIC model. While this is strictly true only for the distribution over an entire basin, rather than a grid cell,

the 100 km × 100 km grid cells we are considering here are sufficiently large that the relationship is still approximately true, i.e. pixels for which a significant fraction of their upslope contributing area lies outside the cell boundaries make up only a small fraction of the grid cell. Figure 1(a) shows the spatial distribution of the topographic wetness index for the study region. Comparison with a map of the region's landcover derived from ALOS/PALSAR imagery (figure 1(b)) reveals a close correspondence between high topographic wetness index values (>14) and the occurrence of bogs.

For each day, the resulting distribution of water table depths is discretized, and methane emissions are estimated for each water table value in the discretized distribution. The total methane emission of the grid cell, then, is the area-weighted sum of the methane emissions from all of the discrete values of the water table depth.

Soil properties were based on typical peat characteristics as outlined in Letts *et al* (2000). Although peat soils only occupy about 37% of the grid cell (based on Sheng *et al* 2004), we nonetheless assume uniform soil properties across the grid cell. Because the sample site is underlain by peat soil, we found it necessary to use peat soil properties to simulate the observed water table drawdown with sufficient accuracy. Since, due to its high porosity, peat soil can accommodate a given change in moisture storage with a smaller change in water table depth than mineral soil, we expect that our estimates of water table variability will be biased downward somewhat for areas of mineral soil. However, the mineral soils in this area are highly correlated with low topographic index values, yielding water table depths that are too deep for substantial methane production. Therefore, this choice should not have much effect on our methane prediction results.

For the VIC and BETHY elements of our model, the plant functional types and area fractions of the grid cell's vegetation tiles were derived from the landcover classification of Hansen *et al* (2000). Vegetation parameters typical of a mix of non-vascular and vascular plants, with a maximum rooting depth of 30 cm, were used for the methane emissions model uniformly throughout the grid cell. The inputs to the models were gridded monthly meteorological forcings based on Adam and Lettenmaier (2007) with daily variability taken from the Sheffield *et al* (2006) data set.

Additional parameters, including the VIC bottom-layer drainage parameters (D_s, $D_{s\,max}$, and W_s), the TOPMODEL scaling factor m, and the methane emission parameters v_{max} and R_0, were calibrated by comparing model results to water table depths and methane fluxes measured at the Bakchar Bog site in 1999 as reported by Friborg *et al* (2003). Gaps in the observed temperature and precipitation records at the site prompted us to use the regional gridded meteorological forcings described above to drive our models for the calibration. Soil column layer thicknesses were set to 0.1 m, 0.4 m, and 2.0 m for the top, middle, and bottom layers, respectively. The resulting simulated and observed 3 cm soil temperatures, water table depths, and methane emissions (figures 2(a), (b), and (c), respectively) matched closely, with the exception of undersimulation of soil temperature in May and undersimulation of methane emissions in September. The

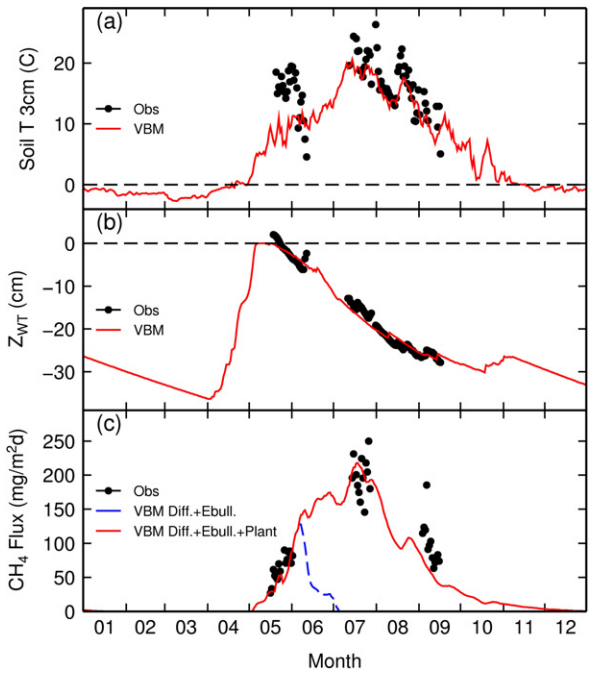

Figure 2. Simulated (labeled as 'VBM' for VIC/BETHY/methane modeling framework) and observed 3 cm soil temperature (a), water table (b), and methane flux (c) at the Bakchar Bog site, 1999. In panel (c), the contribution of diffusion and ebullition pathways to the simulated flux is plotted in the blue dashed line, while the total simulated flux is plotted in the solid red line.

undersimulation of soil temperature in May is likely due to differences between the gridded meteorological forcings and local observations for that summer reported by Friborg *et al* (2003) and Shimoyama *et al* (2003). The underprediction of methane emissions in September may indicate that the model's sensitivity to water table depth is somewhat too high, although the model performance is generally better for other months.

3. Results

To evaluate the ability of our modeling framework to capture interannual variability in methane emissions, we compare simulated and observed soil temperatures, water table depths, and methane emissions for the summers of 1993–1997 at the Bakchar Bog site (figure 3). While the simulated July methane emissions (figure 3(c)) approximate the values of the observed emissions in 1994, 1996, and 1997, large discrepancies exist in July 1993 and 1995, in which observed methane emissions were much higher than in the other years. It is possible that the simulated water table depth (figure 3(b)) in those years is too low. We examined this possibility by prescribing observed soil temperatures and water table depths of 0 cm for the years 1993 and 1995. While this reduced errors somewhat, large discrepancies still remained. Unfortunately observations of the water table depth from most of these years were not available. It should also be noted that, except for 1999, the observed fluxes are the averages over an unspecified number of days, while the model results shown are the average over the entire month of July, which complicates comparisons.

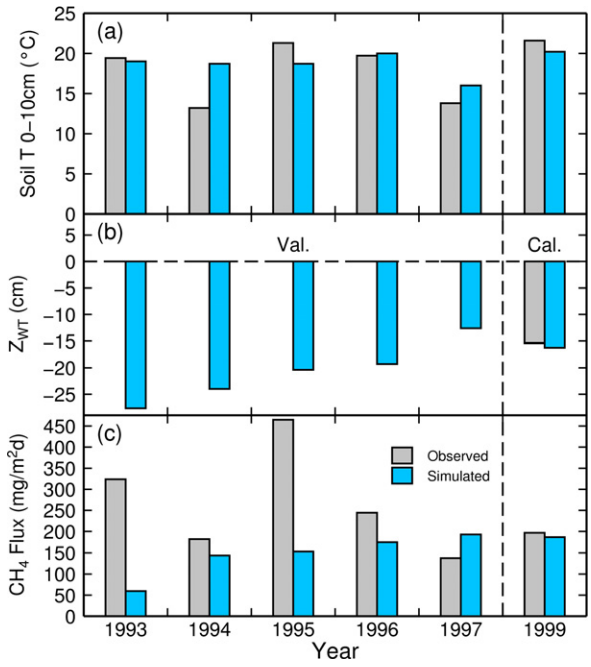

Figure 3. July average simulated and observed (a) soil temperature in the top 10 cm, (b) water table depth, and (c) methane fluxes for the Bakchar Bog site, for the validation years 1993–1997, and calibration year 1999. Observations for years 1993–1997 from Panikov and Dedysh (2000), for an unspecified number of days in July (and August, in the case of 1997). Observations for 1999 from Friborg *et al* (2003) for 14–27 July.

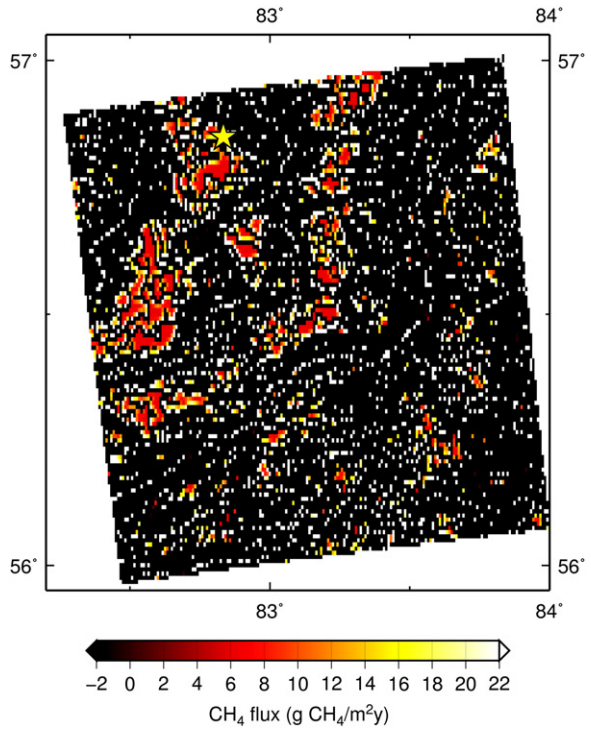

Figure 4. Simulated annual average methane emissions for the 100 km × 100 km grid cell, for the period 1980–1999. The yellow star denotes the Bakchar Bog site.

However, our landscape-scale estimates of methane emissions over the 100 km × 100 km region compare favorably to estimates made by remote sensing and aircraft flyovers. Takeuchi *et al* (2003) extrapolated field observations taken in July 1993 and 1994 to the region bounded by 56–60° N and 78–86° E, using landcover classifications derived from AVHRR and SPOT/HRV images, yielding a regional average July flux of 59.3 mg CH_4 m^{-2} d^{-1} for 1993 and 1994. Meanwhile, estimates of methane fluxes based on vertical profiles from aircraft flyovers in the region in 1994 range from 34 to 126 mg CH_4 m^{-2} d^{-1} (Tohjima *et al* 1994). In comparison, our modeling framework predicts average methane emissions of 43.0 mg CH_4 m^{-2} d^{-1} for the same time intervals. Figure 4 shows a map of simulated average annual methane emissions for the 100 km × 100 km region for the period 1980–1999. The spatial pattern of emissions exhibits a high correlation with the topographic wetness index (figure 1(a)) and wetland vegetation (figure 1(b)). Note that much of the landscape (primarily outside the bogs) actually has a negative methane flux, due to oxidation in the soil; this behavior is typical of non-wetland soils (Nakano *et al* 2004, Crill 1991).

Climate models suggest that northern Eurasia will experience increases in temperature and precipitation by the end of the 21st century (IPCC 2007). In particular, summer temperatures are likely to increase by 2.0–5.6 °C and summer precipitation is likely to change by −1 to +16%, with median values of +3 °C and +9%, or roughly 5–7 mm per month (temperature and precipitation in other seasons may increase even more than this). To investigate the response of wetland water tables and methane emissions to the predicted range of changes in climate, we constructed 24 climate scenarios consisting of the 'baseline' meteorological forcings from 1980–1999 and all 24 combinations of six uniform (year-round) increases in air temperature (0 (1) 5 °C) and four uniform (year-round) increases in precipitation (0 (5) 15%).

Contour plots of the resulting mean annual water table depths, saturated area fractions, and methane emissions, averaged over the 100 km × 100 km grid cell, are shown in figure 5. Some general relationships are evident: increasing temperature and constant precipitation tends to lower the water table (figure 5(a)), reducing the fraction of the grid cell for which soil moisture is at saturation (figure 5(b)), and reducing methane emissions (figure 5(c)), while increasing precipitation, while holding temperature constant, tends to raise the water table, increase the saturated area, and increase methane emissions. One exception to these relationships is for small increases in temperature (1 °C) and precipitation (5%), for which the temperature increase can cause a slight increase in methane emissions.

Results for selected scenarios are given in table 1. For the baseline simulation, average annual methane emissions and water table depth were 1.4 g CH_4 m^{-2} y^{-1} and 108 cm, respectively. For the extreme case of an increase in air temperature of 5 °C methane emissions decreased by 2.1 g CH_4 m^{-2} y^{-1} relative to the baseline, to −0.7 g CH_4 m^{-2} y^{-1}. In this case, methane production in the bogs was less than methane oxidation elsewhere, leading to net consumption of

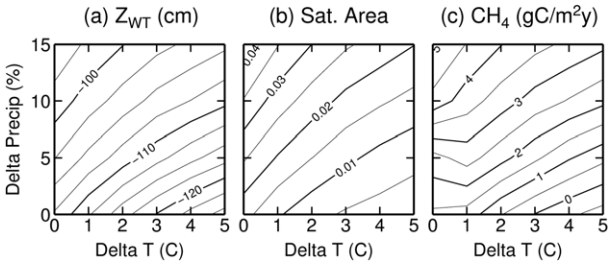

Figure 5. Sensitivity of simulated water table depth (a), saturated area fraction (b), and annual total methane emissions (c), for the 100 km × 100 km grid cell, to changes in temperature and precipitation relative to the 1980–1999 baseline scenario.

Table 1. Simulated average annual methane emissions, water table depths, and saturated areas for various future climate scenarios, compared to current climate baseline. 'T + 5' indicates a uniform 5 °C increase over 1980–1999 temperatures. 'P + 15%' indicates a uniform 15% increase over 1980–1999 precipitation.

Scenario	Annual CH_4 emission (g m^{-2} y^{-1})	Average water table (cm below surface)	Average saturated area fraction
Baseline	1.4	108	0.017
T + 5	−0.7	126	0.002
P + 15%	5.1	96	0.043
T + 5 & P + 15%	3.1	104	0.020
T + 3 & P + 10%	2.8	106	0.019

methane in the grid cell. This reduction was accompanied by a lowering of the water table to 126 cm below the surface. In contrast, increasing precipitation by 15% raised the water table to 96 cm below the surface, which in turn raised methane emissions to 5.1 g CH_4 m^{-2} y^{-1}, a 264% increase relative to the baseline. Combining the increase in temperature and the increase in precipitation ('T + 5 & P + 15%') resulted in intermediate effects: the water table depth (104 cm) remained similar to that of the baseline, and methane emissions rose to 3.1 g CH_4 m^{-2} y^{-1} (or 121% above the baseline). For the median case of an increase in air temperature of 3 °C and an increase in precipitation of 10%, methane emissions increased by 2.8 g CH_4 m^{-2} y^{-1} (or 100% above the baseline) and the water table depth (106 cm) remained similar to that of the baseline.

The mechanisms underlying these results are illustrated in figure 6, which shows the seasonal cycles of relevant variables for the following four scenarios: (1) the current climate baseline, (2) an increase in temperature of 5 °C ('T+5'), (3) an increase in precipitation of 15% ('P + 15'), and (4) increases of 5 °C in temperature and 15% in precipitation ('T + 5 & P+15'). While soil temperature (figure 6(a)) exerts the primary influence on the seasonal evolution of methane emissions (figure 6(f)) within a single year, differences in the annual mean water table depth (figure 6(e)) exert a considerable influence on emissions when comparing different years or climate scenarios. Both air temperature and precipitation determine the seasonal shape and annual mean of the water table depth. The higher air temperatures of the 'T + 5'

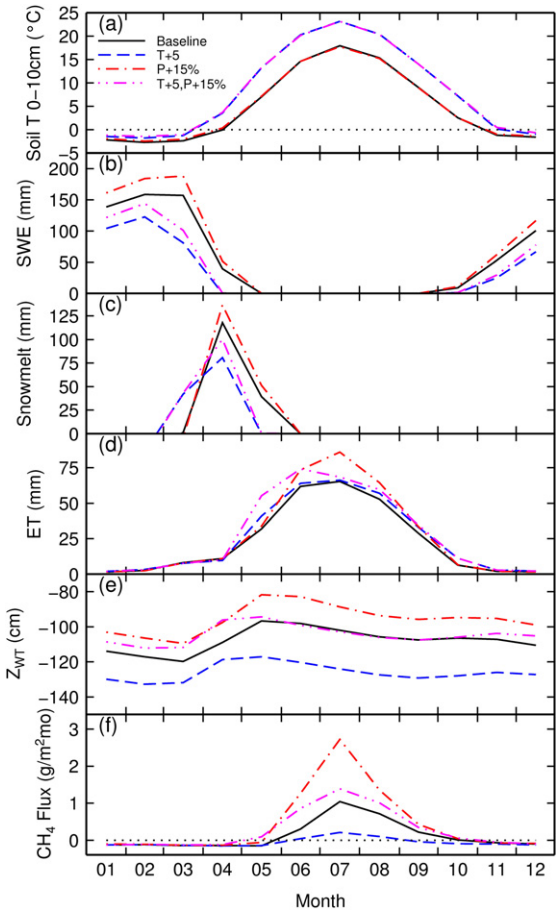

Figure 6. Panels (a) to (f) show monthly average values of soil temperature, snow water equivalent, snow melt flux, evapotranspiration, grid cell-average water table level, and grid cell-average methane emission, respectively, for the 100 km × 100 km grid cell, for the 1980–1999 baseline and for the 'T + 5', 'P + 15%', and 'T + 5 & P + 15%' scenarios for 2080–2099.

and 'T + 5 & P + 15%' scenarios result in smaller snow packs (figure 6(b)) that start and finish melting earlier than the baseline (figure 6(c)), as well as greater evapotranspiration in late spring and early summer (figure 6(d)), leading to lower annual mean water table depths (figure 6(e)). The resulting methane emissions (figure 6(f)) for these scenarios are lower throughout the year than their lower-temperature counterparts (baseline and 'P + 15%', respectively) with the exception of the month of May, when water table depths are at their shallowest and soil temperatures are the limiting factor. On the other hand, the greater precipitation of the 'P + 15%' and 'T + 5 & P + 15%' scenarios results in a larger snow pack (figure 6(b)) and larger peak in snow melt flux (figure 6(c)) but modest change in the timing of melt in comparison with the baseline and 'T+5' scenarios, respectively. Evapotranspiration (figure 6(d)) is also higher in these scenarios, due to greater upper-layer soil moisture. The larger snowmelt pulses and rainfall infiltration lead to higher annual mean water tables (figure 6(e)) and greater methane emissions throughout the

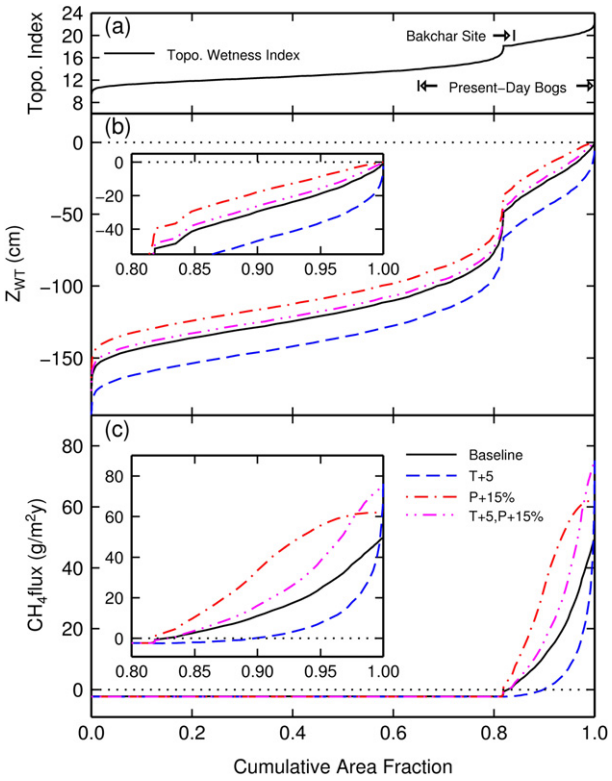

Figure 7. (a) Cumulative distribution of topographic wetness index for the 100 km × 100 km grid cell. The range of wetness index values containing present-day bogs is indicated. Panels (b) and (c) show cumulative distributions of simulated annual average water table level and simulated annual average methane emission, respectively, for the grid cell, for the 1980–1999 baseline and for the 'T + 5', 'P + 15%', and 'T + 5 & P + 15%' scenarios for 2080–2099.

year (figure 6(f)). Thus, the balance between temperature- and precipitation-induced effects on the water table plays a major role in the response of these wetlands to climate change.

These interactions between temperature and precipitation are not uniform across the landscape, as illustrated in figure 7. For reference, figure 7(a) shows the distribution of topographic wetness index as a function of cumulative area fraction within the 100 km × 100 km grid cell. Present-day bogs, indicated on the plot, fall in pixels with wetness index values above 14, with a high concentration above 18. Owing to their higher topographic wetness index values, these pixels tend to have much shallower water table depths than the rest of the grid cell. In the baseline scenario, many of the present-day bog areas (5% of the grid cell) have mean annual water table depths (figure 7(b)) no deeper than 20 cm, and a small portion of these areas are completely saturated (i.e. the water table is at the surface) year round. Accordingly, those bog areas with mean annual water table depths less than 20 cm emit from 20 to 48 g CH_4 m^{-2} y^{-1} (figure 7(c)). Meanwhile, approximately 80% of the grid cell (including some of the bog areas) has water table depths greater than 50 cm, and has a net emission of −2 g CH_4 m^{-2} y^{-1} due to the oxidation of methane in the soil.

In the three future climate scenarios described above, the responses of the water table (figure 7(b)) and methane emissions (figure 7(c)) to changes in climate vary spatially, and in some cases the responses of different regions cancel each other out. In the 'T + 5' scenario, the drop in the grid-cell-average water table causes (a) a reduction in the area of the grid cell that is saturated year round, and (b) a lowering of the local water table in all non-saturated areas. While methane emissions increase up to 75 g CH_4 m^{-2} y^{-1} in the saturated areas due to temperature-driven increases in metabolic activity, emissions decrease elsewhere in response to the deeper water table depths, resulting in a net reduction in methane emissions over the whole grid cell. In contrast, the 'P + 15%' scenario raises the water table in all areas of the grid cell that are not completely saturated in the baseline scenario, increasing emissions throughout the areas with a topographic index >18. In particular, the rise in the water table causes the saturated and near-saturated areas (water table depth shallower than 20 cm), which emit methane at 20 g CH_4 m^{-2} y^{-1} or more, to expand from 5% to 10% of the grid cell area. Finally, in the 'T + 5 & P + 15%' scenario, the higher precipitation approximately cancels the effect of higher temperature on the water table depth, causing water table depths across the grid cell to remain similar to the baseline. While higher temperatures lead to higher peak methane production rates (75 g CH_4 m^{-2} y^{-1}), the increase in methane production rates occurs disproportionately in the saturated areas of the grid cell, due to the shallower water table depths, and thus when summed over the entire grid cell, amounts to a smaller increase in emissions than in the 'P + 15%' scenario. In general, because the distribution of water table depths depends on the shape of the distribution of topographic wetness index, we can expect the net change in methane emissions to vary from region to region as a function of topography.

4. Discussion

From figure 5, we can see that increases in temperature and precipitation can balance each other to some extent, causing some climate scenarios (for example, 'T + 3 & P + 10%' and 'T + 5 & P + 15%') to have similar impacts on regional methane emissions. The most extreme impacts occur for those scenarios involving substantial changes in either temperature alone or precipitation alone. However, these less-balanced scenarios tend to fall on the outskirts of the range of climate predictions (IPCC 2007). Under scenarios closer to mid-range of the IPCC (2007) estimates, regional water table depths would experience modest changes, while methane emissions would increase between 50 and 125% according to our model results.

Our prediction of a 100% increase in annual average methane emissions for the median end-of-century climate scenario ('T + 3 & P + 10%') is consistent with other modeling studies (e.g. Zhuang *et al* 2006, Gedney *et al* 2004, Shindell *et al* 2004) that have predicted substantial increases in methane emissions from northern wetlands under various climate scenarios for the 21st century. Like Shindell *et al*, we find that changes in the extent of saturated and near-saturated area (annual average water table depth shallower than 20 cm) play a large role in the response of wetlands to climate change.

Despite using a similar approach to Gedney *et al*, we find the change in wetland extent to be more important to methane emissions than they did. One reason for this may be that our methane emissions are more sensitive to water table depth than theirs. Another reason may be that we calibrated our models to match local observations, while Gedney *et al* calibrated their model to reflect global atmospheric methane concentrations. More simultaneous observations of water table depth, soil temperature, and methane emissions, over more points across the landscape, would help constrain our models.

Our results also depend in part on the accuracy of our simulated water table depths, which in turn are particularly sensitive to the soil porosity. A higher-porosity soil can accommodate a given change in soil moisture (e.g. due to infiltration or evaporative demand) with a smaller change in water table depth than a lower-porosity soil. In order to preserve the assumptions of the TOPMODEL framework, we have assumed spatially uniform soil properties. In reality, the mineral soils outside present-day bogs tend to have lower peat content, and thus lower porosity than the values we used in our simulations. Therefore, we might expect that the water table will exhibit more variability outside the bogs than we have predicted. On the other hand, these areas also tend to have lower topographic index values, and therefore deeper water table depths and much lower methane production rates, than the bogs, and thus have very little influence on total methane emissions across the landscape. Zhuang *et al* (2006) avoided this problem by prescribing the wetland fraction of each grid cell, and only modeling a uniform water table in the wetland fraction. However, this approach does not consider the non-linear response of methane emissions to heterogeneity in the water table depth and therefore neglects the changes in methane emissions due to changes in the extent of the saturated region. Some combination of these approaches, in which the water table distribution is modulated by local soil properties, could prove useful in this regard.

While we have only considered uniform increases in temperature and precipitation throughout the year, climate models in fact suggest that winter temperature and precipitation will likely increase more than in summer (IPCC 2007). The resulting size and melt dates of the snow pack under these conditions may lead to earlier and larger rises in the water table, which, coupled with higher spring temperatures, could lengthen the duration of substantial methane emissions. It also should be noted that our modeling framework predicts very low methane emissions during the winter. Some field studies have found that winter methane emissions can account for up to 22% of the annual total (e.g. Aurela *et al* 2002, Panikov and Dedysh 2000, Alm *et al* 1999). On the other hand, given that soil temperatures during the winter do not change appreciably among scenarios due to the insulation of the snow pack, and that the snow pack effectively decouples soil moisture from winter precipitation until snow melt, we do not expect winter emissions to be nearly as sensitive to climate change as summer emissions.

Other factors we have not considered include increased atmospheric CO_2 concentrations and changes in nutrient availability. Increased atmospheric CO_2 would likely reduce transpiration somewhat, reducing the summertime drop in the water table and increasing methane emissions during late summer. Increased temperatures and drying of soils could lead to the mineralization and subsequent loss of nutrients from the soil, which could reduce methane emissions. Although we believe that these secondary effects would likely be smaller in magnitude than the primary effects of water table changes that we have modeled, these mechanisms should nonetheless be the focus of future research.

5. Conclusions

We have created a modeling framework for the prediction of regional wetland methane emissions by coupling of the VIC macroscale hydrology model with the BETHY terrestrial carbon model and the wetland methane emissions model of Walter and Heimann (2000), incorporating an implementation of the TOPMODEL concept of sub-grid heterogeneity of the water table. This framework reasonably captures seasonal changes in methane emissions as a function of climate, and makes plausible estimates of methane emissions over large areas. Results from a sensitivity analysis indicate that, for the Vasyugan wetlands in western Siberia, methane emissions may increase by 100% over current values under likely climate conditions at the end of this century. In addition, we have found that the interaction of temperature and precipitation, through their effects on the water table depth, play an important role in determining methane emissions from these wetlands. The balance between these effects varies spatially, and their net effect depends in part on sub-grid topographic heterogeneity. Increases in temperature alone tend to reduce emissions because the lowering of the water table (and reduction of the methane-producing area) in response to smaller snow packs and higher evaporative demand more than compensates for the temperature-driven increase in methane production in those areas that remain relatively wet. Meanwhile, increases in precipitation alone tend to increase methane emissions through the expansion of saturated and near-saturated areas across the landscape. Under conditions of both increased temperature and increased precipitation, the net result depends on the relative strengths of the increases, in addition to the local topography.

Acknowledgment

ALOS/PALSAR imagery of the region was provided courtesy of JAXA.

References

Adam J C and Lettenmaier D P 2007 Application of new precipitation and reconstructed streamflow products to streamflow trend attribution in Northern Eurasia *J. Clim.* at press

Alm J, Saarnio S, Nykänen H, Silvola J and Martikainen P J 1999 Winter CO_2, CH_4, and N_2O fluxes on some natural and drained boreal peatlands *Biogeochemistry* **44** 163–86

Aurela M, Laurila T and Tuovinen J-P 2002 Annual CO_2 balance of a subarctic fen in northern Europe: importance of the wintertime efflux *J. Geophys. Res.* **107** (D21)

Beven K J and Kirkby M J 1979 A physically based, variable contributing area model of basin hydrology *Hydrol. Sci. Bull.* **24** 43–69

Brodzik M J and Knowles K W 2002 EASE-Grid: a versatile set of equal-area projections and grids *Discrete Global Grids* ed M Goodchild (Santa Barbara, CA: National Center for Geographic Information & Analysis)

Brooks R H and Corey A T 1964 Hydraulic properties of porous media *Hydrology Paper no. 3* Civil Engineering Department, Colorado State University

Chen C, Liaw A and Breiman L 2004 Using random forest to learn imbalanced data *Technical Report Series,* Report no. 666, Version 1 Statistics Department, University of California at Berkeley

Christensen T R, Ekberg A, Ström L, Mastepanov M, Panikov N S, Öquist M, Svensson B H, Nykänen H, Martikainen P J and Oskarsson H 2003 Factors controlling large-scale variations in methane emissions from wetlands *Geophys. Res. Lett.* **30** (7) 1414

Crill P M 1991 Seasonal patterns of methane uptake and carbon dioxide release by a temperate woodland soil *Glob. Biogeochem. Cycles* **5** 319–34

Dickinson R E, Henderson-Sellers A, Rozensweig C and Sellers P 1991 Evapotranspiration models with canopy resistance for use in climate models, a review *Agric. For. Meteorol.* **54** 373–88

Dise N B, Gorham E and Verry S 1993 Environmental factors controlling methane emissions from peatlands in Northern Minnesota *J. Geophys. Res.* **98** 10583–94

Famiglietti J S, Devereaux J A, Laymon C A, Tsegaye T, Houser P R, Jackson T J, Graham S T, Rodell M and van Oevelen P J 1999 Ground-based investigation of soil moisture variability within remote sensing footprints during the Southern Great Plains 1997 (SGP97) Hydrology Experiment *Water Resour. Res.* **35** 1839–51

Famiglietti J S, Rudnicki J W and Rodell M 1998 Variability in surface moisture content along a hillslope transect: Rattlesnake Hill, Texas *J. Hydrol.* **210** 259–81

Farquhar G D, von Caemmerer S and Berry J A 1980 A biochemical model of photosynthesis in the leaves of C3 species *Planta* **149** 78–90

Farr T G and Kobrick M 2000 Shuttle radar topography mission produces a wealth of data *EOS Trans. Am. Geophys. Union* **81** 583–5

Food and Agriculture Organization (FAO) 1998 *Digital Soil map of the Word and Derived Soil Properties* [CD-ROM] Land Water Digital Media Ser. 1 Rome.

Friborg T, Soegaard H, Christensen T R, Lloyd C R and Panikov N S 2003 Siberian wetlands: where a sink is a source *Geophys. Res. Lett.* **30** (21)

Gedney N, Cox P M and Huntingford C 2004 Climate feedback from wetland methane emissions *Geophys. Res. Lett.* **31** L20503

Gorham E 1991 Northern peatlands: role in the carbon cycle and probable responses to climate warming *Ecol. Appl.* **1** 182–95

Hansen M C, Defries R S, Townshend J R G and Sohlberg R 2000 Global land cover classification at 1 km spatial resolution using a classification tree approach *Int. J. Remote Sens.* **21** 1331–64

IPCC 2007 *Climate Change 2007: The Physical Science Basis. Contribution of Working Group I to the Fourth Assessment Report of the Intergovernmental Panel on Climate Change* ed S Solomon, D Qin, N Manning, Z Chen, M Marquis, K B Averyt, M Tignor and H L Miller (Cambridge: Cambridge University Press) p 996

Knorr W 2000 Annual and interannual CO_2 exchanges of the terrestrial biosphere: process-based simulations and uncertainties *Glob. Ecol. Biogeogr.* **9** 225–52

Letts M G, Roulet N T, Comer N T, Skarupa M R and Verseghy D 2000 Parameterization of peatland hydraulic properties for the Canadian Land Surface Scheme *Atmos.-Ocean* **38** 141–60

Liang X, Lettenmaier D, Wood E and Burges S 1994 A simple hydrologically based model of land surface water and energy fluxes for general circulation models *J. Geophys. Res.* **99** 14415–28

Matthews E and Fung I 1987 Methane emission from natural wetlands: global distribution, area, and environmental characteristics of sources *Glob. Biogeochem. Cycles* **1** 61–86

Nakano T, Inoue G and Fukuda M 2004 Methane consumption and soil respiration by a birch forest soil in West Siberia *Tellus* B **56** 223–9

Panikov N S and Dedysh S N 2000 Cold season CH_4 and CO_2 emission from boreal peat bogs (West Siberia): winter fluxes and thaw activation dynamics *Glob. Biogeochem. Cycles* **14** 1071–80

Panikov N S, Dedysh S N, Kolesnikov O M, Mardini A I and Sizova M V 2001 Metabolic and environmental control on methane emission from soils: mechanistic studies of mesotrophic fen in West Siberia *Water Air Soil Pollut. Focus* **1** 415–28

Saarnio S, Alm J, Silvola J, Lohila A, Nykänen H and Martikainen P J 1997 Seasonal variation in CH_4 emissions and production and oxidation potentials at microsites of an oligotrophic pine fen *Oecologia* **110** 414–22

Saulnier G-M and Datin R 2004 Analytical solution to a bias in the TOPMODEL framework balance *Hydrol. Process.* **18** 1195–218

Serreze M C, Walsh J E, Chapin F S, Osterkamp T, Dyurgerov M, Romanovsky V, Oechel W C, Morison J, Zhang T and Barry R G 2000 Observational evidence of recent change in the northern high-latitude environment *Clim. Change* **46** 159–207

Shannon R D and White J R 1994 A three-year study of controls on methane emissions from two Michigan peatlands *J. Ecol.* **84** 239–46

Sheffield J, Goteti G and Wood E F 2006 Development of a 50-yr high-resolution global dataset of meteorological forcings for land surface modeling *J. Clim.* **19** 3088–111

Sheng Y, Smith L C, MacDonald G M, Kremenetski K V, Frey K E, Velichko A A, Lee M, Beilman D W and Dubinin P 2004 A high-resolution GIS-based inventory of the west Siberian peat carbon pool *Glob. Biogeochem. Cycles* **18** GB3004

Shimoyama K, Hiyama T, Fukushima Y and Inoue G 2003 Seasonal and interannual variation in water vapor and heat fluxes in a West Siberian continental bog *J. Geophys. Res.* **108** 4648

Shindell D T, Walter B P and Faluvegi G 2004 Impacts of climate change on methane emissions from wetlands *Geophys. Res. Lett.* **31** L21202

Takeuchi W, Tamura M and Yasuoka Y 2003 Estimation of methane emission from West Siberian wetlands by scaling technique between NOAA AVHRR and SPOT HRV *Remote Sens. Environ.* **85** 21–9

Tohjima Y, Maksyutov S, Machida T and Inoue G 1994 Airborne measurement of atmospheric CH4 over the West Siberian Lowland during the 1994 Siberian Terrestrial Ecosystem-Atmosphere-Cryosphere Experiment (STEACE) *Proc. 3rd Symp. on the Joint Siberian Permafrost Studies between Japan and Russia* pp 50–7

Valentine D W, Holland E A and Schimel D S 1994 Ecosystem and physiological controls over methane production in northern wetlands *J. Geophys. Res.* **99** 1563–71

Walter B and Heimann M 2000 A process-based, climate-sensitive model to derive methane emissions from natural wetlands: application to five wetland sites, sensitivity to model parameters, and climate *Glob. Biogeochem. Cycles* **14** 745–65

Zhuang Q, Melillo J M, Sarofim M C, Kicklighter D W, McGuire A D, Felzer B S, Sokolov A, Prinn R G, Steudler P A and Hu S 2006 CO_2 and CH_4 exchanges between land ecosystems and the atmosphere in northern high latitudes over the 21st century *Geophys. Res. Lett.* **33** L17403